Supplementary Material:

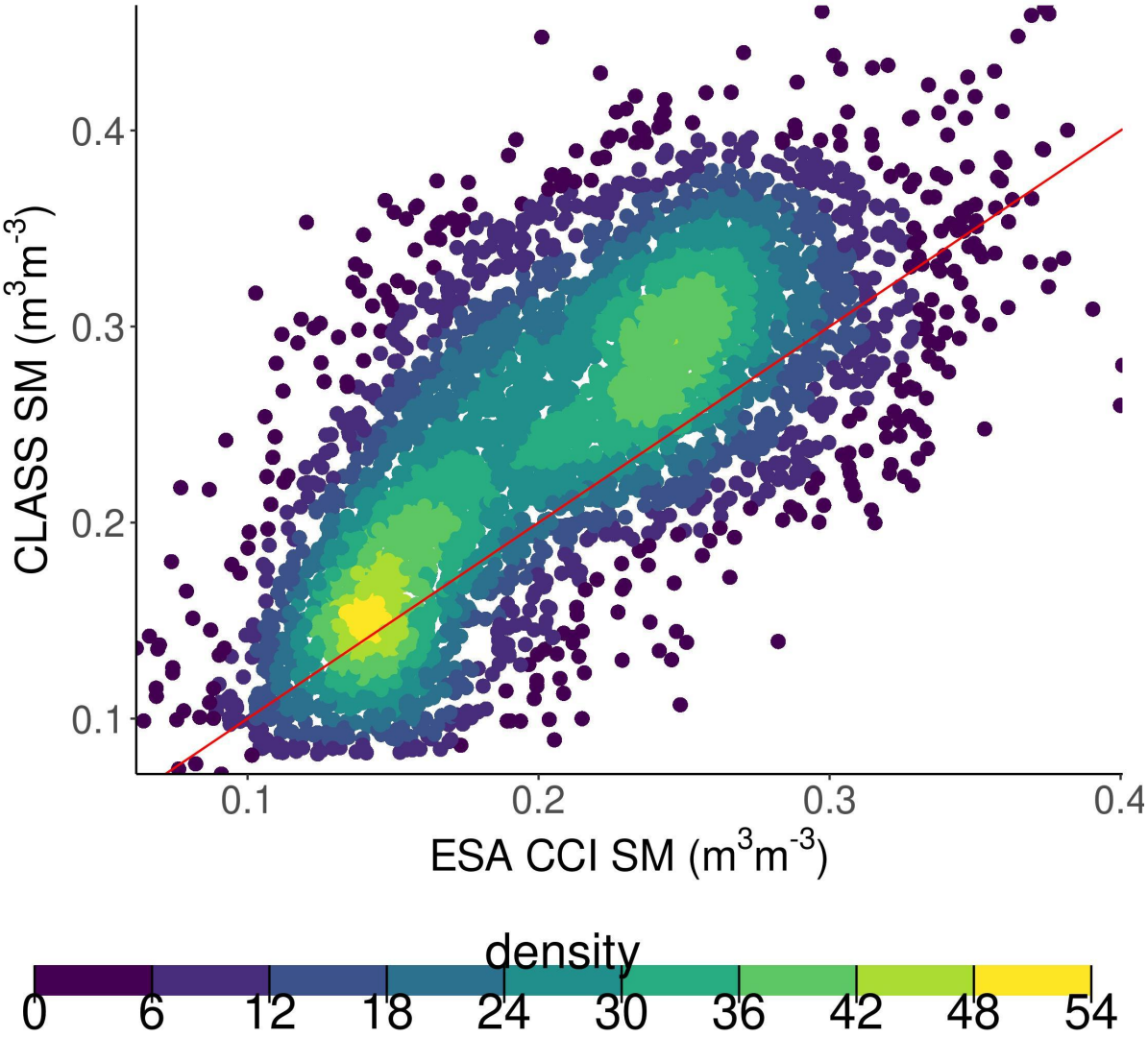

Supplementary Figure 1: Validation of soil moisture fitted with balloon sounding data. The x-axis displays remotely sensed soil moisture from ESA CCI in the 1.0°x1.0° grid cell where sounding data is available. The y-axis displays the soil moisture that was fitted with balloon sounding data and CLASS4GL. The colors denote the density of the scatter points and the red line is the 1:1 line.

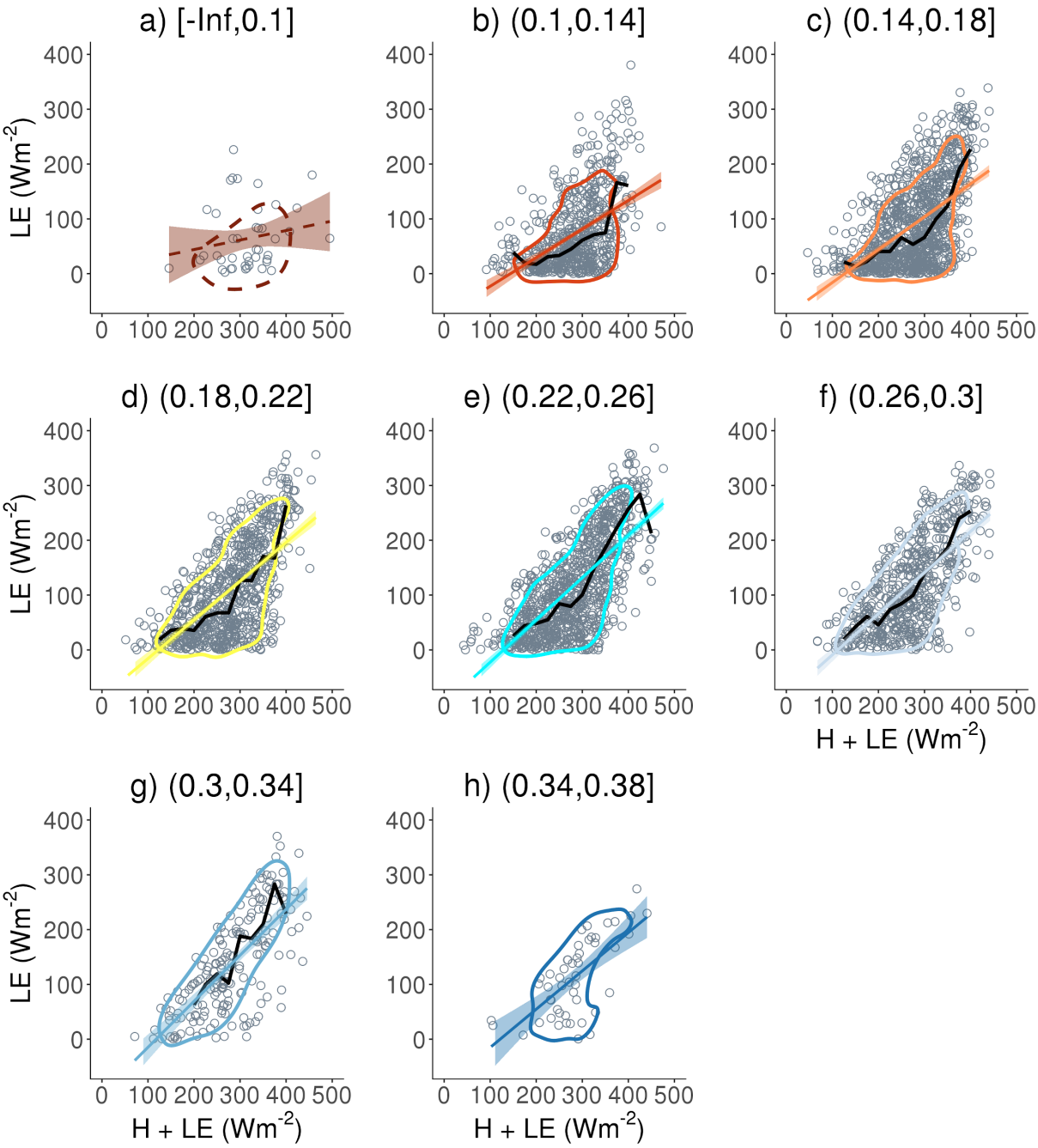

Supplementary Figure 2: Energy flux partitioning per soil moisture class. Available energy (H + LE) and latent heat flux (LE) estimates from all available balloon soundings across stations (points). Point clouds are summarized by 80th percentile contour lines and colored according to respective soil moisture. Least-squares regression fits with corresponding 95% confidence intervals are shown in colored lines. The black lines denote the moving median through the point cloud.

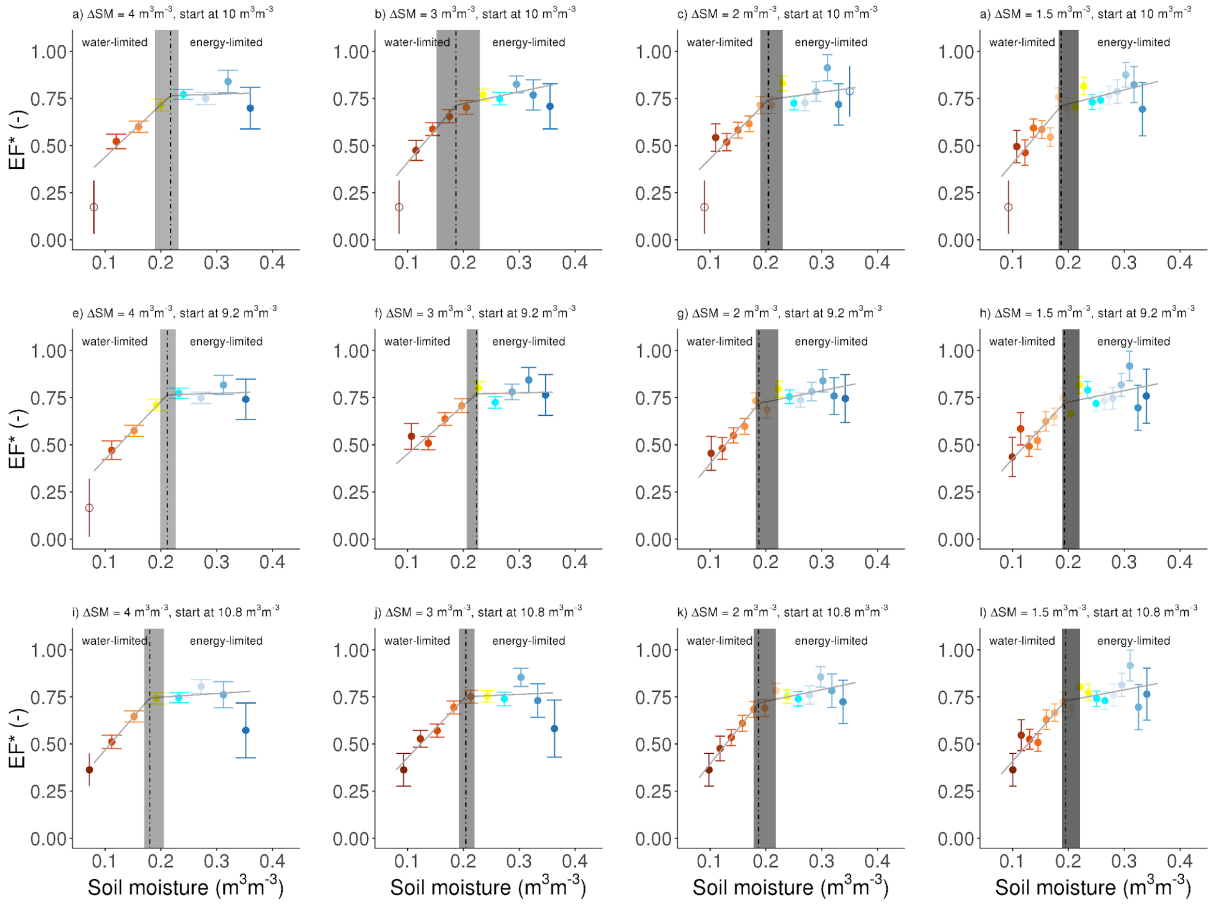

Supplementary Figure 3: Robustness of EF* and piecewise linear regressions with respect to soil moisture class bin width and soil moisture lower boundaries. Relation between the slope of the linear models (EF*) with SM (full dots indicate statistical significance, $p < 0.05$). 4 different bin widths have been used for SM classes: 0.04 m^3m^{-3} (a,e,i), 0.03 m^3m^{-3} (b,f,j), 0.02 m^3m^{-3} (c,g,k) and 0.015 m^3m^{-3} (d,h,l). Different lower boundaries of the SM classes have been used: .1 m^3m^{-3} (top), 0.092 m^3m^{-3} (middle) and 0.108 m^3m^{-3} (bottom). Error bars show the standard deviation of EF*. Dark-grey solid lines result from a piecewise linear regression between SM and EF* with the black dot-dashed line indicating the breakpoint and the light-grey ribbon the respective interquartile range derived with bootstrapping.

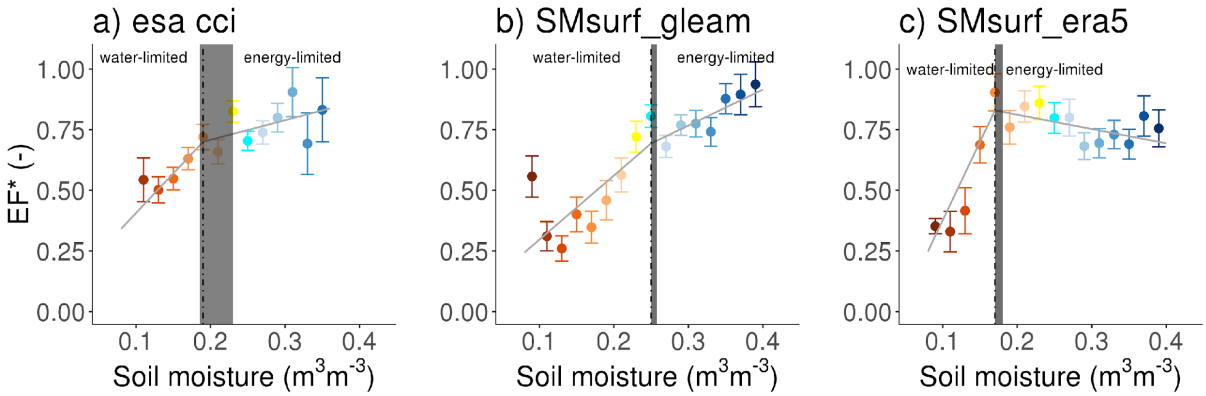

Supplementary Figure 4: Robustness of EF* and piecewise linear regressions according to different soil moisture datasets. Relation between the slope of the linear models (EF*) with soil moisture from ESA CCI (a), GLEAM (b) and ERA5 (c). Solid points depict EF* when $p < 0.05$. Error bars show the standard deviation of the linear models. Error bars show the standard deviation of EF*. Dark-grey solid lines result from a piecewise linear regression between SM and EF* with the black dot-dashed line indicating the breakpoint and the light-grey ribbon the respective interquartile range derived with bootstrapping.

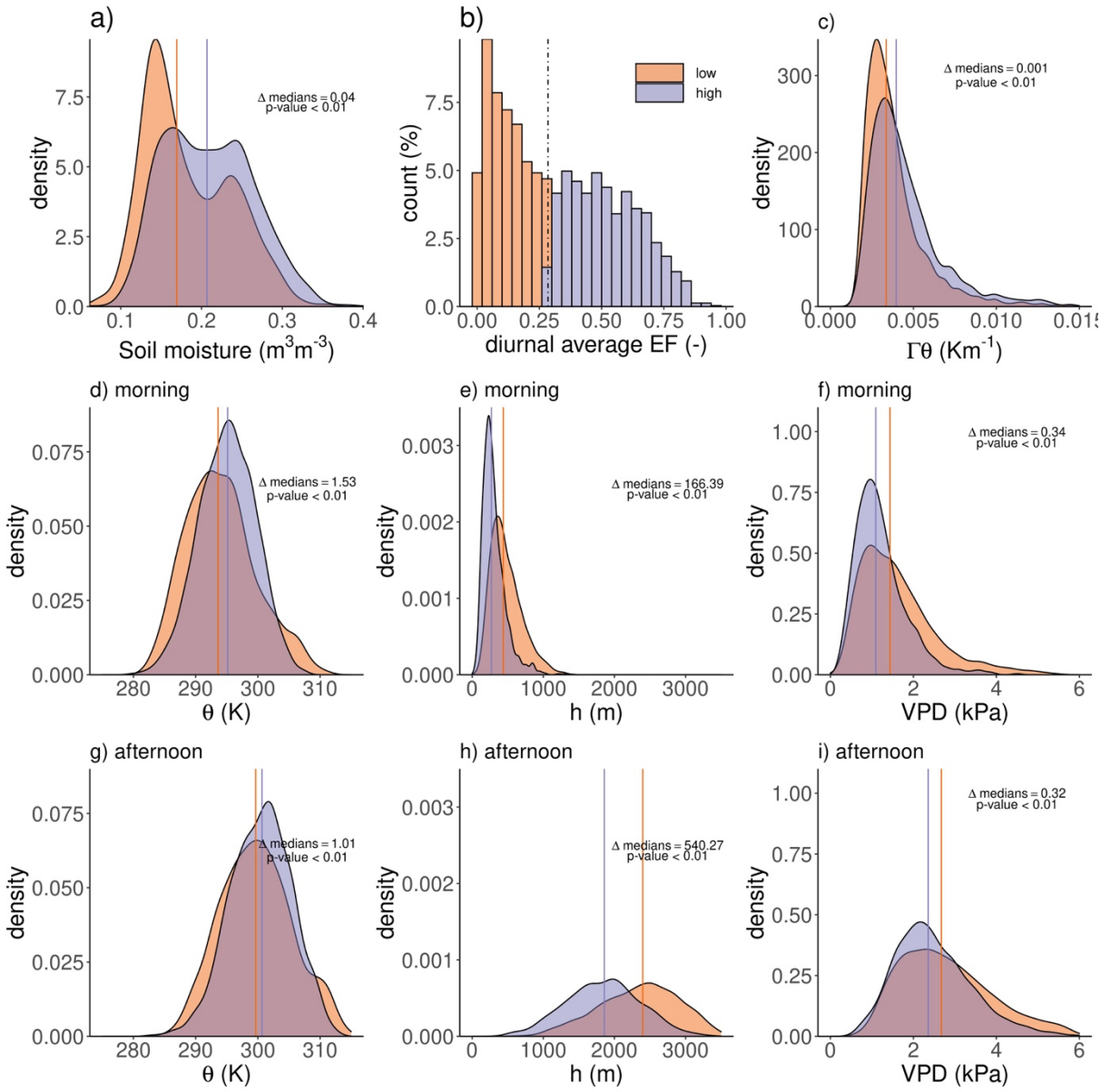

Supplementary Figure 5: Evaporative fraction control on diurnal ABL evolution. Data has been divided into sounding days with a lower (orange) or higher (blue) evaporative fraction (EF) than the median. a) Surface soil moisture for available sounding days from the ESA CCI data set[51]. EF b) and potential temperature lapse rate c) averaged between 08:00 and 14:00 local solar time. Potential temperature (d, g), ABL height (e, h) and the vapor pressure deficit (f, i) at 08:00 and 14:00. Vertical orange and blue lines denote the medians from the respective distributions. Annotations show the difference between the medians and the p-values of the Kolmogorov-Smirnov test.

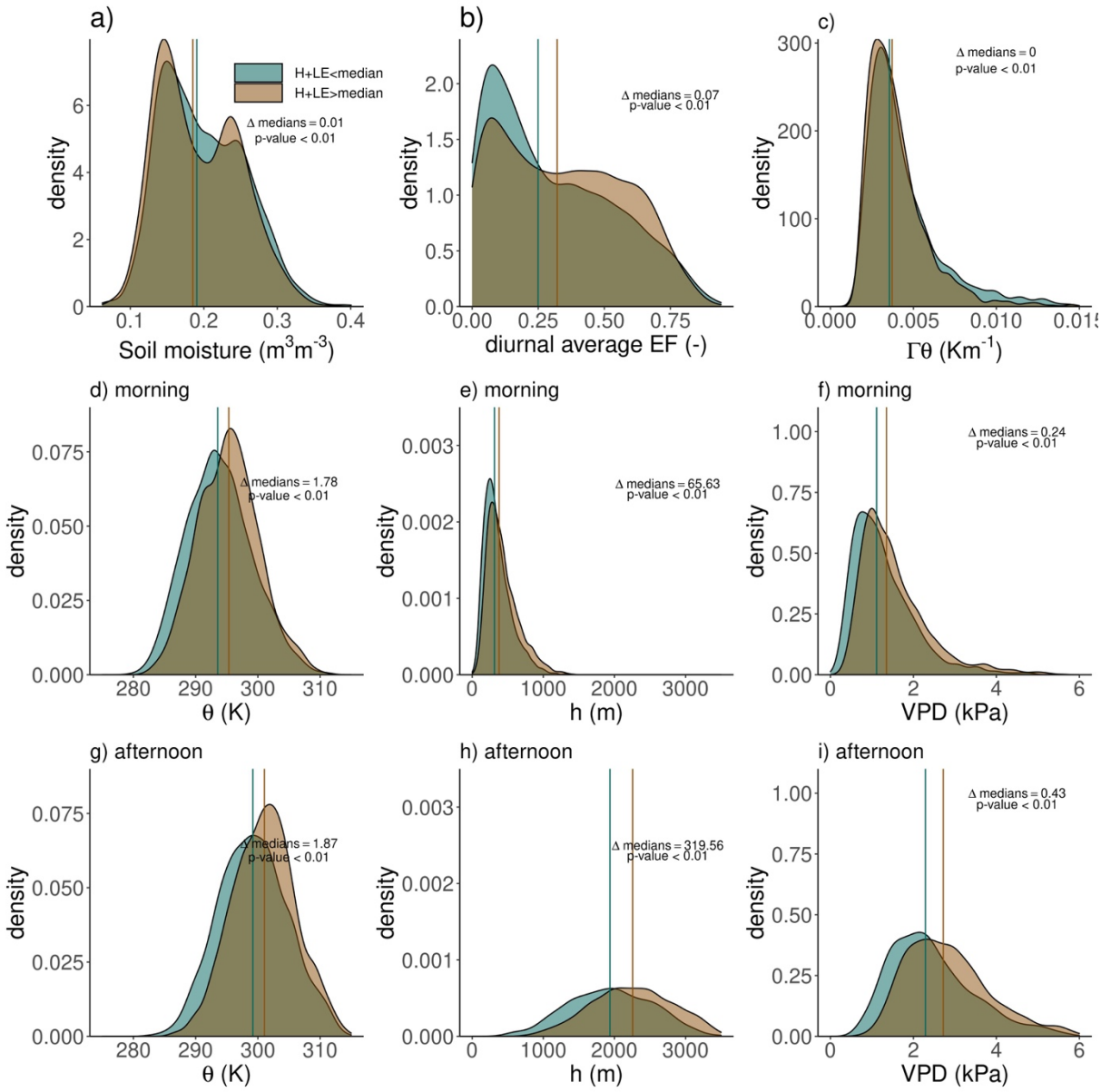

Supplementary Figure 6: The effect of seasonality on diurnal ABL evolution. Data has been divided in sounding days with more (brown) or less (green) available energy (H+LE) than the local median, thereby accounting for latitudinal differences in H + LE. a) Surface soil moisture for available sounding days from the ESA CCI data set[51]. Evaporative fraction b) and potential temperature lapse rate c) averaged between 08:00 and 14:00 local solar time. Potential temperature (d, g), ABL height (e, h) and the vapor pressure deficit (f, i) at 08:00 and 14:00. Vertical brown and teal lines denote the medians from the respective distributions. Annotations show the difference between the medians and the p-values of the Kolmogorov-Smirnov test.